ACADEMIC PRESS

Available online at www.sciencedirect.com
SCIENCE DIRECT®

Journal of Catalysis 215 (2003) 317–325

JOURNAL OF CATALYSIS

www.elsevier.com/locate/jcat

Synergetic effect of gold in Au/Pd catalysts during hydrodesulfurization reactions of model compounds

A.M. Venezia,[a,*] V. La Parola,[b] G. Deganello,[a,b] B. Pawelec,[c] and J.L.G. Fierro [c]

[a] *Istituto per lo Studio dei Materiali Nanostrutturati, ISMN-CNR Sezione di Palermo, via Ugo La Malfa 153, 90146 Palermo, Italy*
[b] *Dipartimento di Chimica Inorganica e Chimica Analitica "S. Cannizzaro," Università di Palermo, Viale delle Scienze, Parco D'Orleans, 90128 Palermo, Italy*
[c] *Istituto de Catalysis y Petroleoquimica, CSIC, Campus UAM, Cantoblanco, 28049 Madrid, Spain*

Received 2 October 2002; revised 18 November 2002; accepted 26 November 2002

Abstract

The simultaneous formation of colloidal dispersions of Pd and Au metal particles protected by the organic polymer polyvinylpyrrolidone (PVP) in reducing alcohol solution was used for the synthesis of new silica-supported monometallic and bimetallic Au_xPd_y catalysts with different x/y ratios. The samples, with a 2 wt% total metal loading, after air calcinations at 673 K to remove the PVP, were characterized by X-ray diffraction, X-ray photoelectron spectroscopy, and FTIR spectra of chemisorbed CO. Formation of alloyed Au_xPd_y particles of different metal composition with consequent modification of their electronic and geometric properties was ascertained. The catalytic activity of the samples as a function of the gold–palladium content was tested in the hydrodesulfurization of thiophene and dibenzothiophene. For the former reaction, performed at low hydrogen pressure, the promoting effect of gold on the palladium activity was confirmed. For the latter reaction, carried out under high hydrogen pressure, pure gold catalyst exhibited larger activity and different selectivity compared to those of pure palladium catalyst. In both reactions the maximum activity was observed in correspondence of the bimetallic sample with 50/50 metal composition. The results are discussed with regard to electronic and ensemble size effects.

Keywords: Au–Pd catalysts; Polyvinylpyrrolidone; Hydrodesulfurization; HDS; Thiophene; Dibenzothiophene

1. Introduction

Noble metal catalysts are widely used in processes of environmental importance such as hydrodesulfurization (HDS) of petroleum feedstocks [1,2], hydrodechlorination from organic molecules [3], NO_x abatement [4], and aromatics hydrogenation [5,6]. With respect to the spreading use of diesel as transportation fuel, high-quality diesel oils are required. According to the new legislation, the specifications of these oil fractions require very low levels of sulfur (< 50 ppm) and aromatics (< 10.0 vol%) [7]. Moreover, it has been shown that a decrease of the aromatic content has a positive effect on the cetane number [8]. The conventional CoMo systems are good HDS catalysts but they allow only a moderate saturation of the polyaromatics to be achieved. They face a series of drawbacks such as initial deactivation by "coke," sintering of the sulfide phases, and difficulty reaching high levels of aromatic saturation due to the thermodynamic constraints of the aromatic saturation at high temperature. However, due to their low cost, they are still the preferred industrial catalysts for HDS.

According to the study by Pecoraro and Chianelli [9], transition metals can be good HDS catalysts as long as they form relatively stable surface complexes characterized by intermediate heat of formation with the organic sulfide substrate. On the basis of the bulk metal–sulfur bond strength, noble metals such as Pd and Pt could be good candidates as HDS catalysts. Moreover, they work at lower temperatures, although they tend to be poisoned by the sulfur present in the feed [7,10,11]. The negative effect of sulfur, causing particle growth, can be alleviated by addition of a second transition metal [12–14].

Based on the above considerations, on recent findings about the capability of Pd to directly activate the thiophene decomposition, and on the particular affinity of gold with sulfur compounds [15,16], a series of Au_xPd_y catalysts sup-

* Corresponding author.
E-mail address: anna@ictpn.pa.cnr.it (A.M. Venezia).

0021-9517/03/$ – see front matter
doi:10.1016/S0021-9517(03)00005-8

ported on silica was prepared and tested in the HDS of thiophene and dibenzothiophene. A recent study in this laboratory [17] has indicated a positive effect of gold on the HDS activity of Pd catalysts supported on amorphous aluminosilicate (ASA). The deposition–precipitation method used for the preparation of the catalysts allowed Au_xPd_y bimetallic particles of rather large size (> 10 nm) and different composition to be obtained. Adopting a new synthesis procedure, in the presence of polyvinylpyrrolidone (PVP) acting as a protective agent against metal sintering [18,19], the present work deals with the study of the HDS behavior of a new series of supported Au_xPd_y catalysts. Silica was chosen as carrier because of its inert character which allows for a better understanding of possible metal alloying effects. The structural and surface characterization of the samples was performed by means of X-ray diffraction (XRD), X-ray photoelectron spectroscopy (XPS), and FTIR spectroscopy of chemisorbed CO. The catalysts were tested in HDS of thiophene and dibenzothiophene to evaluate their activity and selectivity as functions of the metal catalyst composition.

2. Experimental

2.1. Catalyst preparation

Monometallic Pd/SiO_2 and Au/SiO_2 and bimetallic Au_xPd_y/SiO_2 catalysts with total metal loading of 2 wt% were prepared by impregnation of the silica support with an alcohol solution of colloidal dispersion of the two metal particles. Commercial sodium-free SiO_2 was used (Aldrich; surface area 546 m^2/g; pore size 10–50 Å; point of zero charge 3.8). The colloidal dispersions of the Au/Pd clusters protected by the polymer poly(*N*-vinyl-2-pyrrolidone) were obtained by an alcohol-reduction method [18]. 10^{-2} M aqueous solution of tetrachloroauric acid ($HAuCl_4$) and 10^{-2} M ethanol solution of $PdCl_2$ were prepared. Both solutions were mixed in different ratios to obtain the appropriate metal composition. Water or ethanol was added to form a final ethanol/water (1/1 v/v) solution containing the two metals and the PVP (MW = 10,000). The weight ratio of the PVP over the metal precursor was about 5. After adding the silica support to the solution, the suspension was stirred and refluxed at 363 K for 5 h under nitrogen. Darkening of the solution indicated reduction of the metal ions. The excess of liquid was removed in a rotary evaporator and the solid was washed several times to eliminate the free PVP and the chloride ions. Finally the samples were dried in an oven at 343 K and then calcined in air at 673 K for 1 h. At this temperature PVP decomposes completely. All reagents were from Aldrich Chemical Co. The prepared catalysts are labeled as in Table 1. The numbers in the sample notation refer to the relative weight percentages of the metals.

Table 1
Rate constants, k at 613 K, of the silica-supported catalysts in the HDS of thiophene

Catalysts	k (ml/g_{cat} s)
Pd	0.37
$Au_{10}Pd_{90}$	0.29
$Au_{25}Pd_{75}$	0.50
$Au_{50}Pd_{50}$	0.60
$Au_{75}Pd_{25}$	0.53
$Au_{90}Pd_{10}$	0.014
Au	0.004

2.2. Catalyst characterization

2.2.1. FTIR

IR spectra of chemisorbed CO were recorded with a Nicolet 5ZDX Fourier transform spectrophotometer, working with a resolution of 4 cm^{-1} over the entire spectral range and averaged over 100 scans. The samples, in the form of self-supporting wafers (10 mg/cm^2), were reduced in flowing hydrogen at 573 K for 1 h and then outgassed under vacuum at the same temperature for 1 h. After admission of CO at room temperature (30 mbar), the fraction of physically adsorbed molecules was removed by outgassing at room temperature for 15 min. Net infrared spectra of chemisorbed CO were obtained after subtraction of a background spectrum of the solid.

2.2.2. XRD

The X-ray diffraction measurements for the structure determination were carried out with a Philips vertical goniometer using Ni-filtered Cu-K_α radiation. A proportional counter and a 0.05° step size in 2θ, from $2\theta = 30°$ to $2\theta = 50°$, were used. The assignment of the various crystalline phases was based on the JPDS powder diffraction file cards [20]. The obtained XRD profiles were fitted using the software provided with the instrument. From the lattice parameter shifts, calculated from the angular position of the (111) and (200) metal reflections, according to Vegard's law, the molar compositions x and y of the solid solutions Au_xPd_y were obtained [21]. The precision of these calculated values was determined mainly by the error on the lattice parameters and was estimated on the order of 5%. The particle sizes of different phases were calculated from the line broadening of the most intense reflections using the Scherrer equation [22]. Estimated errors on particle sizes and on the relative percentages of the different phases are on the order of 10%.

2.2.3. XPS

The X-ray photoelectron spectroscopy analyses were performed with a VG Microtech ESCA 3000 Multilab, equipped with a dual Mg/Al anode. The spectra were excited by the nonmonochromatized Al-K_α source (1486.6 eV) operated at 14 kV and 15 mA. The analyzer operated in the constant analyzer energy mode. For the individual peak energy regions a pass energy of 20 eV across the hemispheres

was used. Survey spectra were measured at 50 eV pass energy. The sample powders were pelletized and then mounted on double-sided adhesive tape. The pressure in the analysis chamber was in the range of 10^{-8} Torr during data collection. The constant charging of the samples was corrected by referencing all the energies to the C 1s peak at 285.1 eV arising from adventitious carbon. Reference to the internal standard line of the Si 2p of the silica support, set at 103.5 eV, did not produce any difference in the binding energy values. The invariance of the peak shapes and widths at the beginning and at the end of the analyses indicated the absence of differential charging. The peaks were fitted by a nonlinear least square fitting program using a properly weighted sum of Lorentzian and Gaussian component curves after background subtraction according to Shirley [23] and Sherwood [24]. For the exact determination of the Pd $3d_{5/2}$ and Au $4f_{5/2}$ binding energies, the overlapping Au $4d_{5/2}$ and Pd 4s peaks were included in the fitting procedure. The binding energy values are given with a precision of ±0.15 eV. Contact of the samples with air was minimized during sample loading; in particular for the catalysts after the HDS reaction, the sample preparation procedures were carried out inside a nitrogen-filled glove bag.

2.2.4. Activity tests

The hydrodesulfurization of thiophene was carried out in the vapor phase using a continuous-flow microreactor and the analytical setup as described [17]. The reaction conditions were temperature of 613 K, feed mixture of 5.2 vol% of thiophene in H_2 with a flow rate of 25.7 ml/min, and weight hourly space velocity (WHSV) of 7710 h^{-1}. The rate constant was calculated from the integral reactor equation: $k_{HDS} = -\ln(1 - x) \cdot F_0/W$, where x is the fractional conversion at steady state conditions, F_0 (ml s^{-1}) is the volumetric flow of the total reactant gas mixture, and W is the weight of the catalysts (g). Measurements of the rate constants at three different temperatures (613, 628, and 643 K) allowed determination of the activation energy for each catalyst.

HDS of dibenzothiophene (DBT) was performed in a continuous high-pressure down-flow reactor. For the activity tests, the catalyst sample (0.25 g) was dried under a N_2 flow of 100 ml/min for 0.5 h and then activated in a steam of hydrogen (30 ml/min) and nitrogen carrier (50 ml/min) at 573 K for 9 h. After activation, the catalyst's purging at the reaction temperature of 573 K for 15 min was performed. Then, the system was pressurized ($P = 30$ bar) with H_2 and the liquid feed mixture was passed through the reactor. Feed consisted of 1 wt% solution of DBT dissolved in *n*-decaline (Aldrich; 99% purity). Reaction conditions were temperature of 553–593 K, H_2 flow rate of 5.8 l (STP) h^{-1}, and (WHSV) of 35 g of feed h^{-1} per g of catalyst. Activity was measured at three different temperatures, 593, 613, and 633 K, running from the lowest to the highest temperature and maintaining the reaction at each temperature until steady state conditions were reached. Once the reaction was carried out at a given temperature, the next temperature was reached while maintaining the catalyst in a flow of H_2. To check whether there was any deactivation of the catalysts, the activity was checked back at the lowest temperature (553 K) at the end of all the experimental runs. Liquid products were trapped by a condenser at 283 K. Samples were collected periodically and analyzed by GC with FID (Varian chromatograph Model Star 3400 CX) equipped with a 30 m × 0.53 mm DB-1 column (100% methylpolysiloxane, J&W Scientific) as stationary phase, using an initial temperature of 313 K (for 1 min), then heating at a rate of 20 K min^{-1} to 473 K, and holding at that temperature for 5 min. In addition to unreacted DBT, biphenyl (BP) and cyclohexylbenzene (CHB) were the only detected products. Total DBT conversion was calculated as DBT disappearance, and HDS selectivity was defined as (BP)/(CHB + BP) × 100 [25]. Activation energies were obtained from the Arrhenius plots using pseudo first-order rate constant, calculated from steady state conversion of DBT at each temperature.

3. Results

The catalytic results for the HDS of thiophene with regard to the rate constants are reported in Table 1. With the exception of the $Au_{10}Pd_{90}$ and the $Au_{90}Pd_{10}$ samples, the rate constants of the bimetallic palladium catalysts are larger than the rate constant of the monometallic palladium catalyst. The pure gold sample appears to be quite inert. The rate constant increases with increasing loading of gold up to 50 wt%; thereafter it declines with higher gold content. The catalytic test performed on the silica support alone did not show any activity at all. It is worth noticing that after 2 min of time on-stream all the analyzed samples exhibited a 100% conversion of thiophene to something not detectable by the GC and likely to consist of oligomeric by-products [26]. The successive analyses detected unreacted thiophene and C4 products. The activation energies were all of the order of 15 kJ/mol, quite smaller than the activation energies obtained for the same reaction with a series of Au_xPd_y catalysts supported on ASA [17]. Pore diffusion limitation may account for such low values. Indeed the silica used here as support contains a larger fraction of small pores than the previously used ASA [27]. Considering palladium as the active metal and gold as a promoter, the experimental rate constants were normalized with respect to the palladium content [17]. The obtained values were then reported versus gold content as shown in Fig. 1. With increasing amount of gold a steady increase of the rate constant expressed per unit mass of Pd is observed up to the $Au_{90}Pd_{10}$ sample for which a drastic decrease occurred.

The total DBT conversion on monometallic and bimetallic catalysts as a function of temperature is shown in Fig. 2. An increase of the conversion with temperature up to 593 K is observed on all samples except the monometallic Pd on

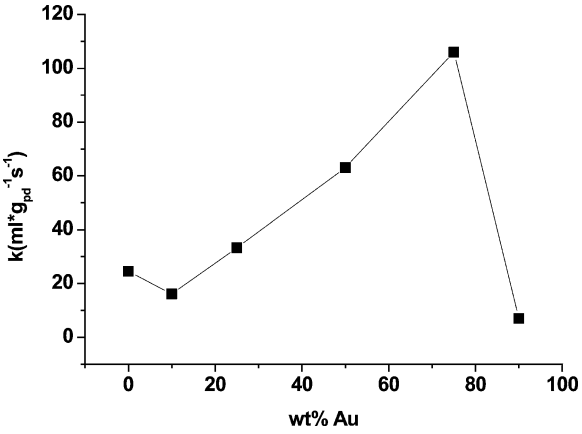

Fig. 1. Thiophene HDS rate constant normalized to palladium weight, as a function of gold loading for the silica-supported Au_xPd_y catalysts. $T = 613$ K.

which constant conversion is observed above 573 K. The results of the catalytic tests are summarized in Table 2 where the activities and selectivities at 593 K and the activation energies are reported. With regard to the selectivities, constant values were obtained at different temperatures and therefore at different conversion rates. In Fig. 3 the total DBT conversion versus the wt% Au is plotted. The following observations arise: (a) pure gold is more active than pure palladium catalyst; (b) as shown in Fig. 3, the total DBT conversion increases from monometallic palladium through the bimetallic catalysts with a volcano-type trend and a maximum of activity in correspondence of the bimetallic sample, $Au_{50}Pd_{50}$; (c) the activation energies change with the catalyst composition, increasing from pure palladium to pure gold catalysts, with a maximum in correspondence of the $Au_{50}Pd_{50}$ catalyst; (d) the selectivity to the biphenyl product is 90% for pure gold catalyst and 67% for pure palladium catalyst; and (e) the bimetallic samples have the lowest selectivity independent of the catalyst composition.

X-ray diffraction patterns of the monometallic and bimetallic catalysts in the range (30–50°) of 2θ are shown in Fig. 4. For the monometallic palladium sample, the (101)

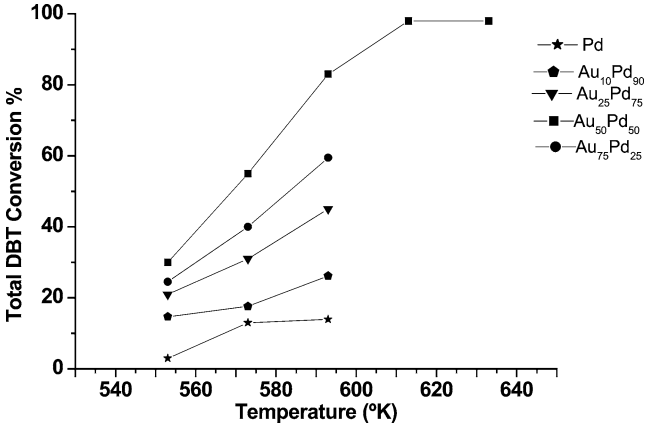

Fig. 2. Dependence of the overall DBT conversion on reaction temperature. $P = 30$ bar; $T = 553$–633 K; WHSV $= 35$ h^{-1}.

Table 2
Total DBT conversion and HDS selectivity as BP/([CHB] + [BP]) obtained at 593 K and activation energies, E_{act}, of the Au_xPd_y catalysts

Catalysts	DBT conv%	$\frac{[BP]}{[CHB]+[BP]}$	E_{act} (kJ mol^{-1})
Pd	13.9	67	29.7
Au_{10} Pd_{90}	21.2	67	43.4
Au_{25} Pd_{75}	44.8	52	62.6
Au_{50} Pd_{50}	83.0	58	128.0
Au_{75} Pd_{25}	59.5	55	78.6
Au	24.3	90.1	80.0

and the (110) reflections of the PdO oxide are present along with a small (111) peak of metallic Pd. The gold catalyst exhibits the most intense reflections, (111) and (200), typical of pure metallic gold. The presence of a broad peak in the diffractograms of the bimetallic samples, centered at a 2θ value intermediate between the (111) of the metallic gold and the (111) of metallic palladium, is an indication of alloy formation. For palladium content above 90 wt% this peak is absent. With increasing gold content, the PdO-related lines decrease in intensity to complete disappearance in the $Au_{75}Pd_{25}$ sample. More detailed analyses of the diffraction patterns, involving fitting of the experimental data and evaluation of the lattice parameters, allowed determination of different Au_xPd_y solid solutions with the corresponding particle sizes and the relative metal percentages. The structural data are reported in Table 3. The compositions of the bimetallic samples on a molar basis are also reported in parentheses in the catalyst column. Solid solutions of different metal composition are formed. The alloyed particles are generally smaller than pure metal particles, and, in particular, an increased amount of palladium in the alloy particles corresponds to smaller particle sizes.

To compare the structural variation undergone by the catalysts during the HDS reaction, the diffractograms of two selected samples, monometallic palladium and bimetallic $Au_{50}Pd_{50}$, in the calcined state and after the HDS of thiophene are shown in Fig. 5. In analogy with recent results on aluminosilicate-supported Au_xPd_y catalysts, the diffractogram of the "aged" pure palladium sample contains

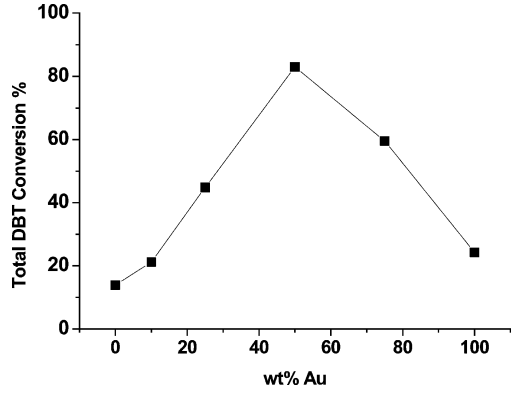

Fig. 3. Total DBT conversion obtained at 593 K as a function of gold content.

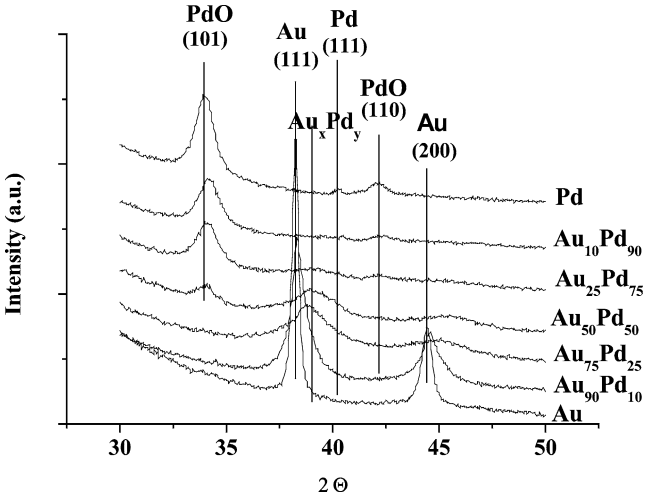

Fig. 4. X-ray diffractograms of monometallic and bimetallic catalysts after calcination at 673 K.

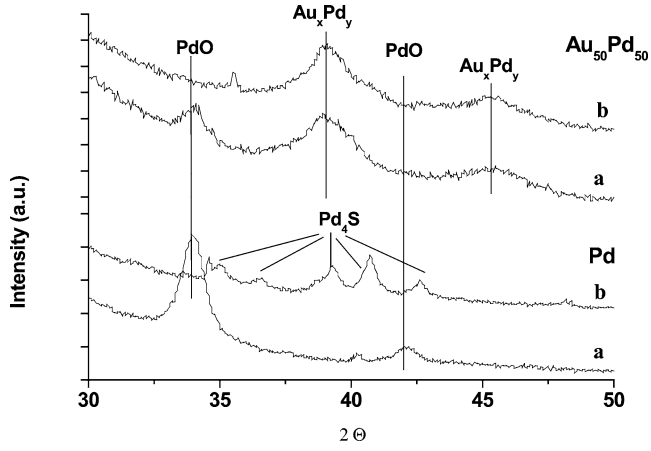

Fig. 5. X-ray diffractograms of monometallic Pd and bimetallic catalyst $Au_{50}Pd_{50}$. (a) After calcinations at 673 K; (b) after HDS of thiophene.

several peaks all arisen from palladium sulfide, Pd_4S [17]. As already pointed out, the preferential formation of Pd_4S would be favored by the low H_2S/H_2 ratio, in accord with the phase diagram of the Pd–S system [17,28]. This sulfide phase is not evidenced in the diffractograms of the bimetallic catalyst, showing that palladium undergoes further reduction, with consequent disappearance of the PdO-related peaks, during the HDS reaction.

The surface properties and the chemical states of the two metals were investigated by X-ray photoelectron spectroscopy. Pd $3d_{5/2}$ and Au $4f_{7/2}$ binding energies along with the XPS-derived atomic ratios of the calcined samples and "aged" samples for HDS of thiophene are reported in Tables 4 and 5, respectively. The corresponding experimental and fitted Pd 3d spectra are shown in Figs. 6 and 7 for some selected samples. In the gold-rich catalysts the wide Au $4d_{5/2}$ peak overlapping with the Pd $3d_{5/2}$ region has also been fitted, taking into consideration its energy and intensity constraints with the Au $4d_{3/2}$ component lying at higher binding energy and not shown in the figures.

The Pd 3d spectra of the calcined samples, shown in Fig. 6, characterized by the two spin-orbit components Pd $3d_{5/2}$ and Pd $3d_{3/2}$ separated by 5.4 eV, exhibit two doublets attributed to two different chemical species. The concentration of each component is affected by the amount of gold. According to the literature, the highest Pd $3d_{5/2}$ energy value (339.4 eV) is attributed to PdO_2, likely formed during air calcination [29]. The component at around 336.5 eV is due to PdO, whereas the component at 335.0 eV is due to metallic palladium [29]. With increasing amount of gold, PdO_2 disappears completely and the metallic palladium peaks increase with respect to those of the PdO species. Gold binding energies are typical of the metallic state [29,30]. A negative shift (0.5–0.8 eV) of the Au $4f_{7/2}$ binding energy for the bimetallic catalysts with respect to the monometallic Au catalyst is observed, in agreement with literature data [17,31]. The shift, attributed to a charge transfer from Pd to Au, possibly increasing the Au *s*-state occupancy, is indicative of alloy formation (ligand effect) [32]. Negative chemical shifts of the Pd 3d binding energy have also been observed in the case of unsupported Pd–Au alloys [32]. However, in the present case, any ligand effect on the palladium binding energies would be masked by the observed shifts mainly due to oxidation state changes (Table 4). As expected for

Table 3
Crystal phases of the mono- and bimetallic samples after calcination at 673 K

Catalysts	Crystal phases (size in Å) %
Au	Au (330) 100%
$Au_{90}Pd_{10}$ ($Au_{84}Pd_{16}$)	Au (270) 51%, $Au_{87}Pd_{13}$ (84) 49%
$Au_{75}Pd_{25}$ ($Au_{62}Pd_{38}$)	$Au_{62}Pd_{38}$ (45) 100%
$Au_{50}Pd_{50}$ ($Au_{35}Pd_{65}$)	PdO (104) 18%, $Au_{47}Pd_{53}$ (39) 82%
$Au_{25}Pd_{75}$ ($Au_{15}Pd_{85}$)	PdO (80) 78%, $Au_{43}Pd_{57}$ (42) 22%
$Au_{10}Pd_{90}$ ($Au_{06}Pd_{94}$)	PdO (81) 100%
Pd	PdO (90) 97%, Pd (242) (3%)

The corresponding crystal particle sizes are given in parentheses with the relative molar percentages. In the first column the composition of the samples on molar basis are also reported.

Table 4
XPS Au $4f_{7/2}$ and Pd $3d_{5/2}$ binding energies (eV) and surface atomic ratios of the catalysts after calcination at 673 K

Sample	Pd $3d_{5/2}$	Au $4f_{7/2}$	$(Au/Si)_{XPS}$	$(Pd/Si)_{XPS}$
Au	–	84.2 (1.8)	0.010	–
$Au_{75}Pd_{25}$	334.9 (2.7)	83.4 (2.2)	0.018	0.021
$Au_{50}Pd_{50}$	334.6 (2.2) (56%)	83.4 (2.2)	0.007	0.068
	336.6 (2.2) (44%)			
$Au_{25}Pd_{75}$	334.5 (2.5) (9%)	83.4 (2.4)	0.005	0.057
	336.5 (2.5) (87%)			
	339.4 (2.5) (4%)			
$Au_{10}Pd_{90}$	336.5 (2.4) (97%)	83.5 (2.0)	0.002	0.070
	340.0 (2.5) (3%)			
Pd	336.5 (2.3) (93%)	–	–	0.077
	339.4 (2.3) (7%)			

The full widths at half maximum are given in parentheses. In the presence of multiple palladium species, the relative percentages of the components are also reported.

Table 5
XPS Au $4f_{7/2}$ and Pd $3d_{5/2}$ binding energies (eV) and surface atomic ratios of the catalysts after HDS of thiophene

Sample	Pd $3d_{5/2}$	Au $4f_{7/2}$	$(Au/Si)_{XPS}$	$(Pd/Si)_{XPS}$
Au	–	83.9 (2.0)	0.006	–
$Au_{75}Pd_{25}$	335.3 (2.5)	83.4 (2.1)	0.008	0.006
$Au_{50}Pd_{50}$	334.9 (2.4)	83.5 (2.2)	0.003	0.045
$Au_{25}Pd_{75}$	335.0 (2.4)	83.2 (2.4)	0.003	0.024
$Au_{10}Pd_{90}$	335.1 (2.5)	83.2 (2.2)	0.002	0.033
Pd	335.0 (2.3) (90%)	–	–	0.033
	337.1 (2.5) (10%)			

The full widths at half maximum are given in parentheses. In the presence of multiple palladium species, the relative percentages of the components are also reported.

impregnated samples, the XPS-derived atomic ratios, Au/Si and Pd/Si, are larger than the nominal ratio.

As reported in Table 5 and as shown in Fig. 7 for the samples after being used in the HDS of thiophene, palladium oxides are reduced to metallic palladium except for a small amount of PdO still present in the monometallic palladium catalyst. Comparing the XPS-derived atomic ratios of Tables 4 and 5, decreases of the Au/Si and, to a large extent, of the Pd/Si atomic ratios are observed upon hydrodesulfurization of thiophene. Analogous results

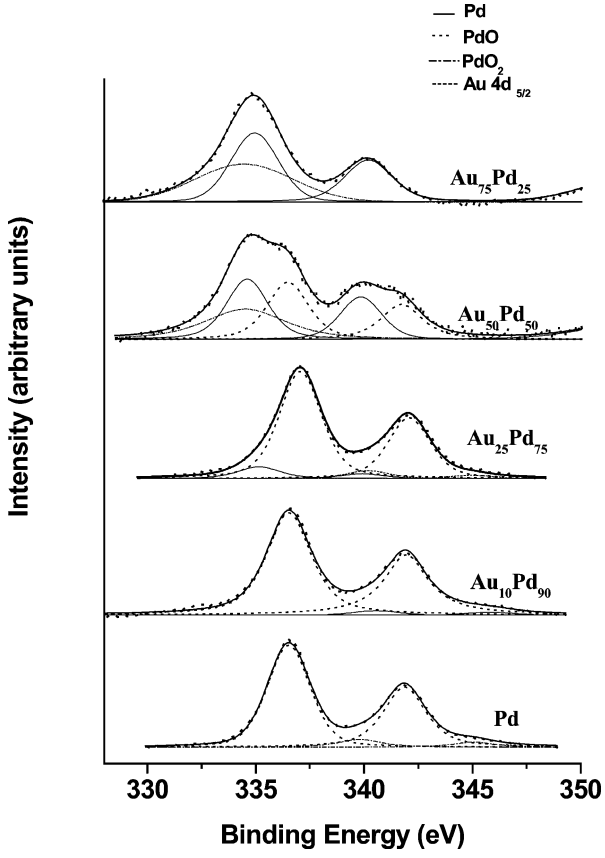

Fig. 6. Pd 3d spectra of monometallic Pd and bimetallic catalysts after calcination at 673 K.

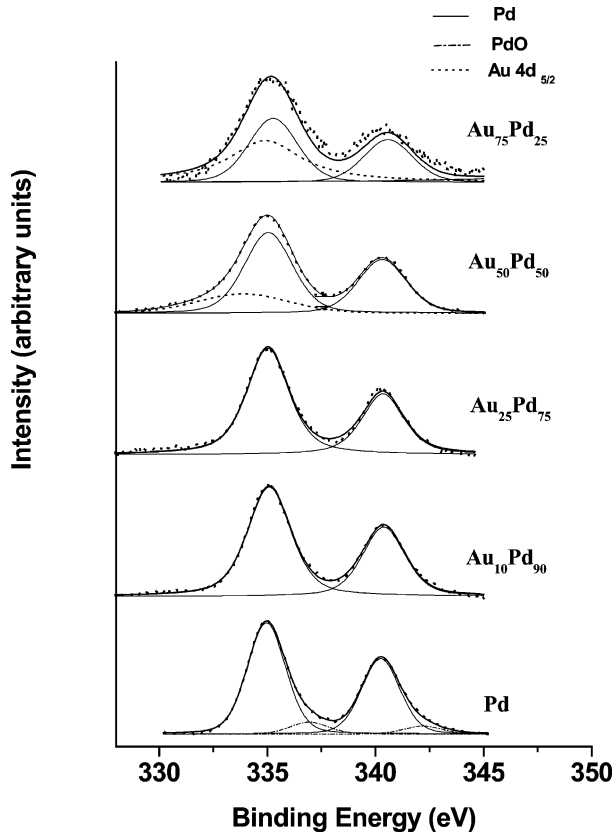

Fig. 7. Pd 3d spectra of monometallic Pd and bimetallic catalysts after HDS of thiophene.

were obtained for the samples after the dibenzothiophene reaction. An increase of the particle sizes upon exposure to the reactant mixture and, for the palladium case, even an inward diffusion of Pd as a consequence of the formation of bulk Pd_4S, revealed by the X-ray diffractograms, could explain the decrease of the atomic ratios.

The FTIR spectra of adsorbed CO were used to identify the surface sites of the Au_xPd_y catalysts. The frequency of the C–O stretching is sensitive to the strength and to the way of bonding. The strength of the bonding is very much related to the electronic structure of the metal. The adsorption modes, such as linear, bridged, and multibonded, depend mostly on geometric factors [33]. The spectra of chemisorbed CO on monometallic palladium and bimetallic Au_xPd_y catalysts are shown in Fig. 8. The monometallic Pd presents two bands at 1998 and 2104 cm^{-1}. The band at the higher frequency is attributed to linearly bonded CO, whereas the band at the lower frequency is due to bridged and multicoordinated CO species [34,35]. For the Pd-free sample two broad bands at 2127 and 2043 cm^{-1} were observed. The former band is due to carbon monoxide reversibly adsorbed on reduced gold sites [36] while the later may arise from multisite adsorption. In accord with previous results on Pd–Au/SiO_2 catalysts, the shape of the spectra of the bimetallic samples change with the amount of gold [36]; the intensity of the high-frequency bands increase

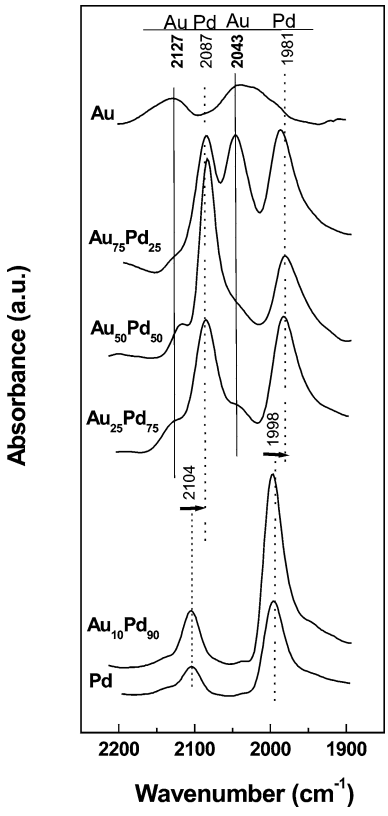

Fig. 8. IR spectra of CO chemisorbed on Pd and Au_xPd_y catalysts after calcinations at 673 K. The samples were outgassed at room temperature after exposure to CO.

at the expense of the intensity of the low-frequency bands. Moreover, the position of the bands are shifted to lower frequencies, to 1981 and to 2087 cm^{-1}. The spectra of gold-rich samples contain a new band at 2043 cm^{-1}.

4. Discussion

Formation of alloyed Au_xPd_y particles in the present series of samples was ascertained by a variety of techniques. Moreover, from the X-ray diffraction patterns the compositions of the solid solutions were obtained. In comparison to a previous series of ASA-supported Au_xPd_y catalysts prepared by a deposition–precipitation method [17] and containing only gold-enriched alloyed particles of rather large size (13–45 nm), the present series, prepared by a newly adopted procedure in the presence of PVP, contains smaller (4–8 nm) alloyed particles of composition close to the nominal one.

Formation of alloys was further confirmed by the FTIR spectra of the irreversible adsorbed CO. The principal linear and multibonded bands of the CO on monometallic Pd catalyst were found to shift to low frequencies and to change their relative intensity upon increase of the gold amount in the bimetallic catalysts. The effect of gold was twofold [34,36]: (a) it contributes to reduce the multibonded CO, with respect to the linearly bonded CO, probably by a geometric rate, that is, decreasing the size of the metal ensemble needed for multiple bonding, and (b) it determines a small gain of d electrons in the adsorbing palladium through the ligand effect [32] and, by enhancing the back-donation to the antibonding π orbitals of CO, causes the low-frequency shift of the stretching vibrations. Moreover, the appearance of the new band at 2043 cm^{-1} could be attributed to linearly adsorbed CO on new adsorption sites formed in the bimetallic clusters. From the catalytic results, shown in Table 1, obtained from the hydrodesulfurization of thiophene, a positive effect of gold on the HDS activity of the silica-supported palladium catalysts was found, in accord with a recent study on the ASA-supported Au_xPd_y samples [17]. However, larger activities relative to those of the previous study [17] were obtained here. Considering that both supports, silica and ASA, were demonstrated to be inert for this type of reaction, the improved activity of the present catalysts can be attributed to the adopted preparation method, which allowed better dispersal of alloyed particles.

As already suggested, the enhanced HDS activity of the Au_xPd_y catalysts can be related to the formation of solid solutions, given in Table 3. It should be remarked that, even though the data of Table 3 refer to the catalysts in the precursor stage, that is after calcinations, they can still be related to the catalytic behavior since, as pointed out previously, the catalyst hydrogen pretreatment did not produce changes of the alloy structure except for a further reduction of the palladium oxide [17]. Moreover, as already determined in the previously mentioned study and as indicated by the X-ray diffractograms of the "aged" samples shown in Fig. 5, the increased activity of the bimetallic catalyst could also be due to the inhibition of the sulfide phase, Pd_4S, by gold.

In relation to the catalytic behavior tested in the HDS of dibenzothiophene, a substantial increase of the activity is obtained in the bimetallic Au_xPd_y catalysts with respect to the pure Pd catalyst. As observed in Table 2 the total DBT conversion increases by a factor of 6 when going from pure Pd to $Au_{50}Pd_{50}$ and the pure gold is even more active than the pure palladium catalyst. Again, the resistance of gold to the sulfur poisoning, as revealed by the absence of sulfide phases in the gold-rich samples, can explain the activity results. As observed in Table 2, gold exhibits larger HDS selectivity with respect to the monometallic palladium catalyst. Considering that no intermediate hydrogenated products such as tetrahydrodibenzothiophene are observed, the mechanism for the hydrodesulfurization may involve a hydrogenation of the rings as a first step followed by rapid C–S bond rupture. This would determine a low biphenyl selectivity. An alternative pathway would consist of a direct S-extrusion leading to the formation of biphenyl. On the basis of the stronger adsorption of the dibenzothiophene with respect to the biphenyl, the subsequent hydrogenation of BP to cyclohexylbenzene is unlikely [37]. The BP/(CHB + BP) ratio can then be taken as a measure of the two pathways, the intermediate hydrogenation and the direct sulfur extru-

sion. The lower BP selectivity of the pure palladium catalyst is in accord with its well-documented hydrogenation activity. On the other hand, the largest selectivity of the gold catalyst is an indication of its poor capability to activate the hydrogen molecule. The surprisingly good activity exhibited by the monometallic gold catalyst in the hydrodesulfurization of dibenzothiophene, in contrast with the almost inertness exhibited in the HDS of thiophene, is likely to be due to the different hydrogen pressure used for the two catalytic tests. In the case of the thiophene reaction, performed at atmospheric pressure, the strong affinity of gold toward the substrate molecule would determine a low hydrogen surface coverage. In the case of the dibenzothiophene reaction, the high H_2 pressure would increase the hydrogen surface coverage, allowing for the hydrogen activation. The C–S bond of the substrate molecule, strongly bound to the gold sites, would then be broken with consequent formation of H_2S. The trend in the activation energies listed in Table 2 are also interesting. The highest values are obtained for the more active catalysts. Increased surface coverage of DBT on gold-enriched samples and different catalytic sites existing in the alloyed phases could determine the observed activation energies. The present results confirmed a beneficial effect of gold, acting as a promoter of palladium catalysts in the low-hydrogen-pressure reaction of thiophene. The effect is likely to be due to the stronger resistance of gold to sulfur poisoning and to the "ensemble" size change of the alloyed phase. Moreover, a synergetic effect between gold and palladium seems to exist in the bimetallic Au_xPd_y catalysts and has been evidenced in the HDS of dibenzothiophene at elevated hydrogen pressure. The synergy of the alloyed particles arises from the strong affinity of gold with the sulfur-containing substrate and from the strong activation of the hydrogen molecule by palladium. By properly tuning the Au/Pd weight ratio it is possible to optimize the reaction with regard to activity and selectivity. Finally, although it is hard to consider gold an ingredient of new catalysts for HDS and hydrogenation reactions, the information provided here may be relevant for the understanding and development of Pd-based catalysts for one- or two-step deep HDS/dearomatization processes of diesel fuels.

5. Conclusion

This study has confirmed the beneficial effect of gold in silica-supported Au_xPd_y catalysts in the HDS reaction of different substrates, under two different experimental conditions. The effect is attributed to formation of Au_xPd_y alloy particles which are characterized by stronger resistance to sulfur poisoning with respect to the pure palladium catalyst and by synergetic influence between the two metals in close contact. By comparing the behavior of the catalysts in the hydrogenation of thiophene at low H_2 pressure and the hydrogenation of DBT at high H_2 pressure, a possible mechanism for the HDS on this type of catalyst would involve a strong attack of the substrate to the gold or palladium sites followed by the C–S rupture activated by the hydrogen.

Acknowledgments

Support by the European Community, Grant COST, Project D 15, is acknowledged. B.P. acknowledges financial support from the Spanish Ministry of Science and Technology through the Ramon y Cajal program.

References

[1] R. Navarro, B. Pawelec, J.L.G. Fierro, P.T. Vasudevan, Recent Res. Dev. Catal. 1 (1996) 7.
[2] W. Qian, Y. Yoda, Y. Hirai, A. Ishihara, T. Kabe, Appl. Catal. A 184 (1999) 81.
[3] M. Bonarowska, J. Pielaszek, W. Juszczyk, Z. Karpinski, J. Catal. 195 (2000) 304.
[4] A.O. Bamwenda, A. Ogata, J. Oi, S. Kushiyama, K. Mizuno, J. Mol. Catal. A 126 (1997) 151.
[5] H. Yasuda, T. Kameoka, T. Sato, N. Kijma, Y. Yoshimura, Appl. Catal. A 185 (1999) L99.
[6] A. Corma, A. Martinez, V. Martinez-Soria, J. Catal. 169 (1997) 480.
[7] B.H. Cooper, B.B.L. Donnis, Appl. Catal. A 137 (1996) 203.
[8] G.H. Unzelman, NPRA Annual Meeting, Paper AM 87-33, March 1987.
[9] T.A. Pecoraro, R.R. Chianelli, J. Catal. 67 (1981) 430.
[10] J. Barbier, E. Lamy-Pitara, P. Marecot, J.P. Boitiaux, J. Cosyns, F. Verna, Adv. Catal. 37 (1990) 279.
[11] J.C. Rodriguez, J. Santamaria, A. Monzon, Appl. Catal. A 165 (1997) 147.
[12] M. Vaarkamp, J.T. Miller, F.S. Modica, G.S. Lane, D.C. Koningsberger, J. Catal. 138 (1992) 675.
[13] C.-A. Jan, T.-B. Lin, J.-R. Chang, Ind. Eng. Chem. Res. 35 (1989) 3893.
[14] Y. Yoshimura, H. Yasuda, T. Sato, N. Kijma, T. Kameoka, Appl. Catal. A 207 (2001) 303.
[15] T.E. Caldwell, I.M. Abdelrehim, D.P. Land, Surf. Sci. 367 (1996) L26.
[16] G.C. Bond, D.T. Thompson, Catal. Rev.-Sci. Eng. 41 (1999) 319.
[17] A.M. Venezia, V. La Parola, V. Nicolì, G. Deganello, J. Catal. 212 (2002) 56.
[18] N. Toshima, M. Harada, Y. Yamazaki, K. Asakura, J. Phys. Chem. 96 (1992) 9927.
[19] F. Bonet, V. Delmas, S. Grugeon, R. Herrera Urbina, P.-Y. Silvert, K. Tekaia-Elhsissen, Nanostruct. Mat. 11 (1999) 1227.
[20] JCPDS Powder Diffraction File Int. Centre for Diffraction Data, Swarthmore.
[21] A.R. West, Solid State Chemistry and its Applications, Wiley, Chichester, England, 1998.
[22] H.P. Klug, X-ray Diffraction Procedures for Polycrystalline and Amorphous Materials, Wiley, New York, 1954.
[23] D.A. Shirley, Phys. Rev. B 5 (1972) 4709.
[24] P.M.A. Sherwood, in: D. Briggs, M.P. Seah (Eds.), Practical Surface Analysis, Wiley, New York, 1990, p. 181.
[25] P.T. Vasudevan, J.L.G. Fierro, Catal. Rev.-Sci. Eng. 38 (1996) 161.
[26] Y. Jin, A.K. Datye, E. Rightor, R. Gulotty, W. Waterman, M. Smith, M. Holbrook, J. Maj, J. Blackson, J. Catal. 203 (2001) 292.
[27] A.M. Venezia, F. Raimondi, V. La Parola, G. Deganello, J. Catal. 194 (2000) 393.
[28] E.J.M. Hensen, H.J.A. Brans, G.M.H.J. Lardinois, V.H.J. de Beer, J.A.R. van Veen, R.A. van Santen, J. Catal. 192 (2000) 98.

[29] Chastain (Ed.), Handbook of X-Ray Photoelectron Spectroscopy, Perkin–Elmer, Eden Prairie, MN, 1992.
[30] D. Dalucu, J.E. Klemberg-Sapieha, L. Martinu, Surf. Sci. 472 (2001) 33.
[31] S. Deki, K. Akamatsu, Y. Hataneka, M. Mizuhata, A. Kajinami, Nanostruct. Mat. 11 (1999) 59.
[32] P.A.P. Nascente, S.G.C. de Castro, R. Landers, G.G. Kleiman, Phys. Rev. B 43 (1991) 4659.
[33] V. Ponec, G.C. Bond, Stud. Surf. Sci. Catal. 95 (1995) 206.
[34] Y. Soma-Noto, W.M.H. Sachtler, J. Catal. 34 (1974) 162.
[35] A.M. Venezia, L.F. Liotta, G. Deganello, P. Terreros, M.A. Peña, J.L.G. Fierro, Langmuir 15 (1999) 1176.
[36] E.L. Kugler, M. Boudart, J. Catal. 59 (1979) 201.
[37] H. Topsoe, B.S. Clausen, E. Massoth, in: J.R. Anderson, M. Boudart (Eds.), Hydrotreating Catalysis, Springer, Berlin, 1996.